Taylor & Francis
Taylor & Francis Group

Sliding mode control of a pneumatic muscle actuator system with a PWM strategy

Ville T. Jouppila[a]*, S. Andrew Gadsden[b], Gary M. Bone[b], Asko U. Ellman[a] and Saeid R. Habibi[b]

[a]Department of Engineering Design, Tampere University of Technology, Tampere, Finland; [b]Department of Mechanical Engineering, McMaster University, Hamilton, Ontario, Canada

In this paper, a sliding mode control (SMC) strategy is applied to a pulse width modulation (PWM)-driven pneumatic muscle actuator system using high speed on/off solenoid valves. Servo-pneumatic systems with PWM-driven on/off valves can be used instead of expensive servo valves to decrease complexity, weight, and cost of servo-pneumatic systems. Due to the highly nonlinear nature of pneumatics, the system is difficult to model accurately which leads to un-modelled dynamics and uncertainties. In this paper, a robust and nonlinear SMC approach is implemented in order to control the system with sufficient accuracy. A nonlinear model is developed in a single-input single-output form by studying the flow, pressure, and force dynamics of the system. The SMC strategy is applied to three different system configurations: single on/off valve, two on/off valves, and a servo valve. The performance and effectiveness of these configurations are investigated under sinusoidal tracking at different frequencies. The robustness of the controllers is studied by varying the inertia of the system and by applying external disturbances to the system.

Keywords: pneumatic actuator; sliding mode control; solenoid valves; pulse width modulation

1. Introduction

Pneumatic systems have many properties that make them attractive for use in a variety of environments. They are less sensitive to temperature than hydraulic systems and it is not necessary to collect exhaust air which removes the need for fluid return lines. In addition, high force-to-weight ratios, cleanliness, compactness, ease of maintenance, and the safety of pneumatic actuators offer desirable features for many industrial designs. Pneumatic McKibben muscle actuators, invented by Gaylord (Gaylord, 1958), provide a higher force-to-weight ratio compared with pneumatic cylinders. However, there are a number of nonlinearities present that makes it rather difficult and complex to model effectively.

Nonlinear characteristics of the actuator, air compressibility, friction, and nonlinear airflow through the valves are the main reasons that pneumatic systems are commonly avoided for advanced applications. Literature demonstrates that a large number of control strategies have been proposed to handle the effects of the nonlinearities present. These include the following: PID control (Chou & Hannaford, 1996), adaptive control strategies (Caldwell, Medrano-Cerda, & Goodwin, 1995; Lilly J., 2003; Medrano-Cerda, Bowler, & Caldwell, 1995), nonlinear PID (Than & Ahn, 2006), neural networks (Hesselroth, Sarkar, Van der Smagt, & Schulten, 1994), and fuzzy controllers (Lilly J., 2003; Medrano-Cerda, Bowler, & Caldwell, 1995; Chan, Lilly, Repperger, & Berlin, 2003; Balasubramanian & Rattan, 2003). In (Lilly & Yang, 2005) and (Carbonell, Jiang, & Repperger, 2001), a sliding mode control (SMC) strategy was

applied to a muscle actuator system, but only simulation results of the effectiveness of the strategy were presented. Other SMC approaches are presented in (Tondu & Lopez, 2000; Aschemann & Schindele, 2008; Shen, Nonlinear Model-Based Control of Pneumatic Artificial Muscle Actuator Systems, 2010). In (Tondu & Lopez, 2000), modelling and control of pneumatic muscle actuators in an antagonistic configuration for a 2-DOF SCARA-type robot prototype was studied. The system was controlled by a sliding mode control strategy based on an identified 2nd order model, from pressure input to joint angle. An additional integrative term in the close neighbourhood of desired angle position was used to improve the tracking accuracy. A static joint accuracy of ±0.2°, and mean dynamic accuracy of ±0.5° for a trapezoidal velocity profile (0.5 rad/s cruising speed and a 0.5 rad/s² slope) was reported. In (Aschemann & Schindele, 2008), a cascaded SMC scheme was presented for a pneumatic linear actuator. A guided carriage was driven by a nonlinear mechanism consisting of a rocker with an antagonistic pair of pneumatic muscle actuators arranged at both sides. The differential flatness of the system was exploited in combination with sliding mode techniques to stabilize the error dynamics in view of un-modelled dynamics. The internal pressure of each pneumatic muscle was controlled by a fast underlying control loop. The control of the outer control loop involved a decoupling of rocker angle as well as mean internal pressure of both pneumatic muscles as flat outputs. Additionally, model uncertainties such as friction were directly counteracted by an observer-based disturbance compensation which

reduces the chattering problem. Experimental results emphasize the excellent closed-loop performance with maximum position errors of approximately 3.5 mm during the movements, negligible steady-state position error, and a steady-state pressure error of less than 0.03 bar.

In the most recent work (Shen, Nonlinear Model-Based Control of Pneumatic Artificial Muscle Actuator Systems, 2010), an SMC strategy was applied to control a muscle actuator system in an opposing pair configuration using a proportional flow control valve. Experimental results with sinusoidal tracking (with amplitude 7.5 mm and frequency 0.5 – 1.5 Hz) showed accuracies of ±0.5 mm to ±1.2 mm. This work and previous SMC studies have demonstrated that it is an efficient and robust control strategy for pneumatic actuator applications. However, in these studies, a proportional or servo valve has been used to control the actuator. In this paper, on/off valve(s) are chosen for the control of the muscle actuator system in order to provide a low cost alternative to servo valve-based pneumatic systems.

In recent years, effort has been made to develop inexpensive servo-pneumatic systems using on/off solenoid valves with pulse-width modulation (PWM). Previous efforts have shown the potential of PWM-controlled pneumatics; although they typically lack an analytical approach when studying the system (Lai, Singh, & Menq, 1992; Noritsugu, 1986; Morita, Shimizu, & Kagawa, 1985). In one article, the nonlinearities of the system were handled by proposing a switching controller based on a reduced order nonlinear model of the system (Paul, Mishra, & Radke, 1994). In (Ahn & Yokota, 2005), a modified PWM valve pulsing algorithm was developed. The proposed algorithm (with a continuous state feedback controller) was successfully implemented, and demonstrated its effectiveness on pneumatic cylinder experiments. In (Van Varseveld & Bone, 1997), a controller based on discrete-time control methods was developed for a PWM-controlled pneumatic servo system. A PID controller with friction compensation and a position feed-forward term was successfully implemented with a worst case steady-state error of 0.21 mm and S-curve trajectory following errors of less than 2.0 mm. In (Barth, Zhang, & Goldfarb, 2003), a linear state-space averaged model and an SMC with a PWM strategy based on a loop shaping approach was introduced for the control of a single degree of freedom pneumatic positioning system with a cylinder. This was followed by a nonlinear averaging approach (Shen, Zhang, Barth, & Goldfarb, 2006) where originally discontinuous and possibly non-affine system in the input was transformed into equivalent continuous-time nonlinear system (that was also affine in control input) for which SMC strategy could be applied. Their approach was demonstrated with a pneumatic cylinder controlled by a pair of 3-way solenoid valves. Sinusoidal tracking with amplitude of 20 mm and frequencies 0.25 – 1 Hz reportedly had accuracies from ±1 mm to ±3.5 mm. In (Nguyen,

Leavitt, Jabbari, & Bobrow, 2007), a SMC strategy using four low cost solenoid valves without PWM to control a double-acting cylinder was introduced. The sinusoidal tracking error for a stroke of ±20 mm at 0.5 Hz was less than 2 mm.

The aforementioned studies of pneumatic PWM on/off valve systems applied their approaches to systems with pneumatic cylinders. However, in this paper, a pneumatic muscle actuator which differs significantly from the traditional cylinder is used. Due to highly nonlinear characteristics of the muscle actuator, a significant effort is applied for modeling the actuator. In addition, previous studies like (Shen, Zhang, Barth, & Goldfarb, 2006) have assumed a linear relation between duty ratio and effective valve opening area, combined with traditional mass flow rate models with choked and un-choked flow. In order to better approximate the mass flow rate through the valve, this paper utilizes a nonlinear continuous model where the mass flow rate is described as a 2nd order bi-polynomial function of actuator pressure and PWM duty ratio. Being a continuous and invertible function, the actual PWM duty ratio control signal for the valve(s) can be solved based on the knowledge of actuator pressure and desired mass flow rate given by the SMC controller output. As a result, the mass flow rate model can be separated from the control law and the system model can be given in a SISO control canonical form for which the SMC strategy can be easily applied.

Most studies lack a thorough review of PWM on/off valve systems and comparisons with proportional/servo valve systems. This paper provides an experimental study of PWM on/off valve systems, including a study of system robustness. A comparative study between on/off valve approaches and traditional servo valve approach is performed.

In this paper, the muscle actuator system shown in Figure 1 is studied. Three different valve configurations will be implemented separately. An SMC strategy will be designed for each configuration and the resulting closed-loop performances compared. The actuator is a Festo fluidic muscle (MAS10-300). It is mounted horizontally and attached to a pneumatic cylinder (Festo DNC-40) whose pressure is controlled by an electronic regulator to provide an adjustable unidirectional returning force for the muscle. Note that the cylinder adds frictional uncertainties for the system that the control strategy needs to compensate. In the first system configuration, a single 3/2 high-speed on/off solenoid valve (Festo MHE2-MS1H-3/2G-M7, cost: $50 USD) drives the muscle actuator. The valve is controlled by varying the duty ratio of a PWM signal. In the second system configuration, two 2/2 solenoid valves (Festo MHE2-MS1H-3/2G-M7 with third port plugged) are used to control the inflow and outflow independently. For comparison purposes, a servo valve (Festo MPYE-5-M5-010-B, cost: $450 USD) is also used to control the actuator in the third system architecture, denoted Case 3 in Figure 1. The controller is programmed in the Matlab
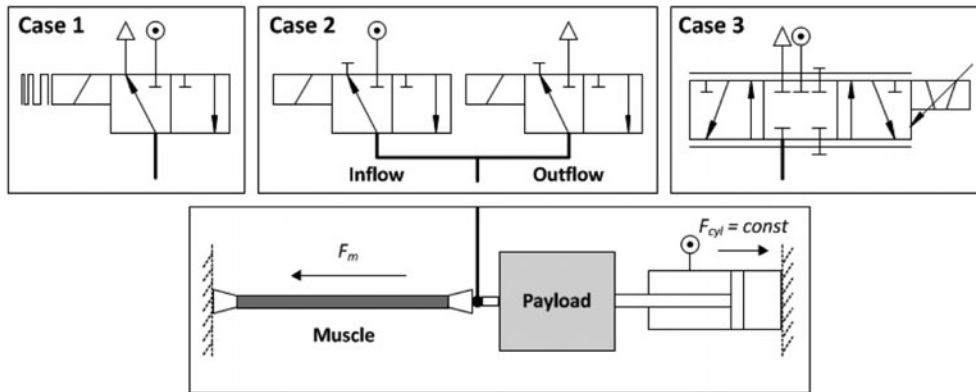
Figure 1.   Muscle actuator system with three different valve configurations.

Simulink environment and is implemented using the Real-Time Windows Target. The controller output signal is transmitted to an electronic amplifier that supplies sufficient power to actuate the valve. The muscle pressure and the displacement of the actuator are measured using Festo SDE1 pressure sensors, and a linear potentiometer, respectively. The velocity and acceleration are obtained by differentiation of the position signal with a digital Butterworth low-pass filter.

As the system under study is highly nonlinear, a simulation model is needed for the initial tuning process and studying the performance of the controller. In Section 2 a nonlinear system model is presented which takes into account the flow, pressure, force, and load dynamics covering the main nonlinearities present in the system. In Section 3, a model-based SMC strategy is designed. Section 4 discusses the tuning of the controller, and compares the performance of the SMC strategy with three different valve configurations. Section 5 presents the conclusions of the research.

2.   Muscle actuator system modelling

This section describes the modelling of the system; including the experimental setup, pneumatic muscle actuator, pressure and valve flow dynamics, and the overall system model in single-input single-output (SISO) form.

2.1   *Pneumatic muscle actuator*

The pneumatic McKibben muscle actuator consists of a rubber tube covered with a double helical braid (Schulte, 1962). During pressurization, the muscle increases in diameter and shortens in length. The maximum force is obtained at the beginning of the contraction and decreases with increasing contraction. The actuator is unidirectional and its maximum contraction is typically 20% to 25% of the nominal length. The advantage of the muscle actuator over the traditional cylinder is the higher force-to-weight ratio and the stick-slip free motion at low velocities. However, the force-to-contraction relationship at different pressure levels is highly nonlinear, and adds to the difficulty of modelling the muscle

actuator effectively. As with all actuation systems, the effective application of the pneumatic muscle actuator relies on being able to accurately model and predict the forces that will be generated under any operating condition.

Figure 2 illustrates the measured nonlinear relationship between the force, pressure, and displacement. Note that the actuator introduces a significant hysteresis phenomenon due to material deformations and the presence of friction. The hysteresis is difficult to model accurately, especially during the transition phase when the direction of the movement changes. In this study, a simple model of hysteresis is used where a force offset is added to the mean static force curve. In this case, the hysteresis can be considered as static Coulomb friction.

The mean static force shown in Figure 2(a) is the averaged force from the upper and lower curves of the hysteresis force loop. The shape of the curves is quite
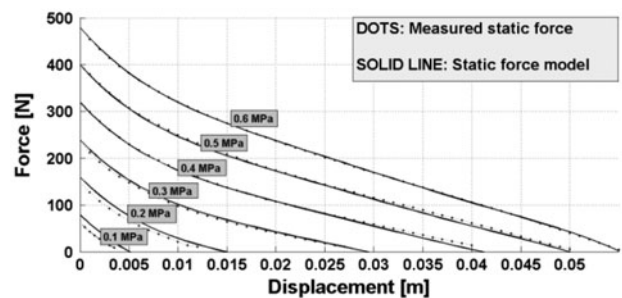
(a) Mean static muscle force characteristics
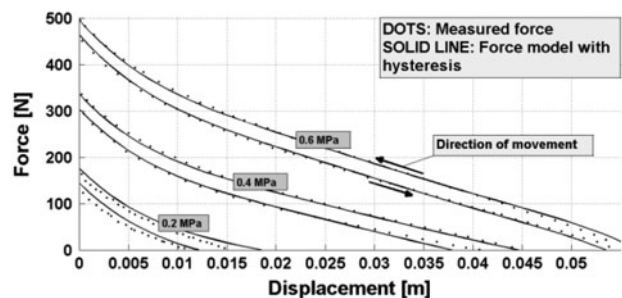
(b) Force model including hysteresis

Figure 2.   Modelling of the muscle static force.

similar for different pressures, and can be captured accurately by fitting a third-order polynomial function $F_{max}(x)$ for the curve at the maximum actuator pressure 0.6 MPa, where x is the contraction/displacement of the muscle.

In order to model the force at different pressure levels, a force term that is subtracted from the maximum possible force is needed. Note that the force is proportional to the pressure when the actuator length is fixed. However, the proportionality factor decreases as contraction increases. This results in the last term in the overall muscle force equation, defined as follows:

$$F_m(x, p_m) = F_{max}(x) - (p_{max} - p_m)(k_0 - k_1 x)$$
$$F_{max}(x) = a_0 + a_1 x + a_2 x^2 + a_3 x^3 \tag{1}$$

where p_{max} is the maximum muscle pressure, p_m is the actual muscle pressure, and a_{0-3}, k_0, and k_1 are the fitted model parameters.

Figure 2 illustrates that the model is able to describe the mean static force-pressure-displacement behaviour with good accuracy. By also including a static Coulomb friction term, the hysteresis effect can be captured reasonably well as shown in Figure 2(b). The viscous friction of the actuator is extremely difficult to determine and model accurately, as it is dependent on the velocity as well as the pressure in the actuator. In this paper a constant damping factor B is used to approximate the viscous friction. In the SMC design described in Section 3, the discontinuous static and Coulomb friction are treated as a disturbance.

2.2 Pressure Dynamics

For calculating the pressure inside the muscle, it is assumed that air is an ideal gas with an adiabatic process such that the change of pressure is as follows:

$$\dot{p}_m = \frac{kRT}{V_m(x)} \dot{m}_{eq}(u_{duty}, p_m) - \frac{kp_m}{V_m(x)} \frac{dV_m(x)}{dx} \dot{x} \tag{2}$$

where k (1.4 for adiabatic process), R, T, and V_m denote the specific heat ratio, gas constant, air temperature, volume of the muscle, and muscle pressure, respectively. The equivalent mass flow rate $\dot{m}_{eq}$ is a function of the PWM duty ratio u_{duty} and actuator pressure p_m, and will be determined in the next section. An empirical linear approximation is used to describe the volume of the muscle actuator as a function of displacement, as follows (Jouppila, Gadsden, & Ellman, 2010):

$$V_m(x) = v_0 + v_1 x \tag{3}$$

where v_0 and v_1 are fitted parameters.

2.3 Valve Mass Flow Rate Dynamics

The mass flow rate model of the 3/2 valve controlling the muscle actuator is an essential part of the system model. The switching frequency f_{PWM} and u_{duty} determine how long the valve is open and closed during the time PWM period ($1/f_{PWM}$). The PWM switching frequency has a significant effect on the system performance as the final control signal for the valve is updated at the implemented PWM frequency. In other words the sampling frequency is equal to the PWM frequency. A small PWM frequency results in poor tracking precision since the sampling frequency should be significantly higher than the natural frequency of the system. However, the switching delay (about 2 ms) sets the limit to the maximum reasonable PWM frequency.

Due to the PWM switching, two modes exist in the system. During the on-mode the valve charges the muscle actuator, and during the off-mode the actuator is discharged. In addition, the flow can be either choked or un-choked depending on the ratio of downstream and upstream pressure. Assuming an ideal gas law and an adiabatic process, a widely accepted model for mass flow rate through the valve is expressed as follows (Pneumatic Fluid Power, 2005):

$$\dot{m} = \begin{cases} Cp_{up}, & \frac{p_{down}}{p} \leq b \\ Cp_{up}\sqrt{1 - \left(\frac{\frac{p_{down}}{p_{up}} - b}{1 - b}\right)^2}, & \frac{p_{down}}{p_{up}} > b \end{cases} \tag{4}$$

where C is defined as the valve conductance and b is the critical pressure ratio. While the valve is open the air flows into the actuator, and the upstream pressure is defined by $p_{up} = p_s$ (supply pressure) and the downstream pressure is $p_{down} = p_m$. While the valve is closed, the air flows out of the actuator, $p_{up} = p_m$ and $p_{down} = p_0$ (atmosphere pressure), respectively. In order to identify the pneumatic behavior of the valve, a set of experiments were carried out according to the procedure introduced by ISO6358 (Pneumatic Fluid Power, 2005). The two parameters (C and b) were found by using Equation (4) with a least squares fitting method for measured data with upstream pressure 0.7 MPa. These results are found in Table 1.

The RMS fitting error for upstream pressure 0.7 MPa was 0.252×10^{-4} kg/s or 0.9% (flow path 1-2) of the range and 0.212×10^{-4} kg/s or 0.7% (flow path 2-3). Figure 3 shows a relatively good overlap also for upstream pressures 0.6 and 0.5 MPa. Note that this flow model combined with valve switching delays is used in

Table 1. Identified parameters for mass flow rate model.

Parameter	Description	Value
p_{up}	Upstream pressure	$0.5, 0.6, 0.7$ MPa
C_{in}	Sonic conductance for charging	$3.48 \times 10^{-3} \frac{\text{kg}}{\text{sMPa}}$
C_{out}	Sonic conductance for discharging	$3.77 \times 10^{-3} \frac{\text{kg}}{\text{sMPa}}$
b_{in}	Critical pressure ratio for charging	0.39
b_{out}	Critical pressure ratio for discharging	0.28
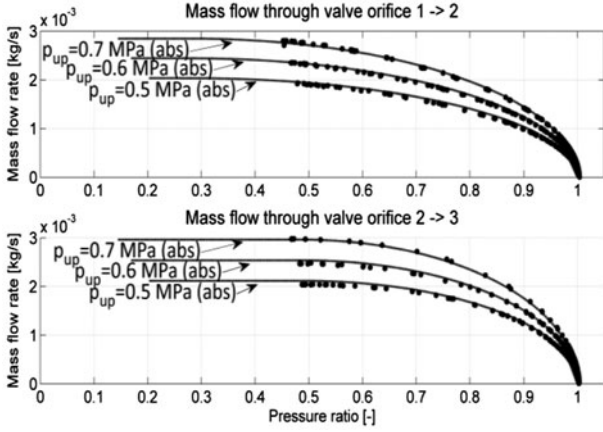
Figure 3.   Mass flow rate model (based on ISO6358).

the simulation study for the initial tuning of the controller parameters.

(i) System with One 3/2 Valve

The discontinuous switching between the on-mode and off-mode is difficult to handle in terms of controller design. An alternative approach introduced in (Jouppila, Gadsden, & Ellman, 2010; Rao & Bone, 2008) is employed to provide a continuous and invertible flow model for the proposed controller design. In order to obtain a precise valve mapping, a pressure response curve was measured while inflating and deflating a closed chamber while operating the valve with different duty ratios. By differentiating the filtered pressure curve and using Equation (2) for a constant volume, the mass flow rate can be approximated. The nonlinear characteristics of the mass flow rate can be captured by the following second-order bi-polynomial function (see details in (Jouppila, Gadsden, & Ellman, 2010)):

$$\dot{m}_{eq}(u_{duty}, p_m) = m_1 + m_2 p_m + m_3 p_m^2 + m_4 u_{duty}$$
$$+ m_5 u_{duty} p_m + m_6 u_{duty} p_m^2 + m_7 u_{duty}^2$$
$$+ m_8 u_{duty}^2 p_m + m_9 u_{duty}^2 p_m^2 \qquad (5)$$

The parameters of (5) were determined using nonlinear least squares. The maximum fitting error was 1.96×10^{-4} kg/s or 4.13% of the range. The RMSE was 5.5×10^{-5} kg/s or 1.16%.

(ii) System with Two 2/2 Valves

Similar valve modelling approaches can be used for determining the flow characteristics in the case where two 2/2 valves are used to control the actuator. The first valve is used for controlling the inflow, and the second for the outflow. With this configuration, unnecessary valve switching can be avoided when the state of the system is close to the desired state (by closing both valves). This helps to save energy and increases the lifetime of the valves.

(iii) System with Servo Valve

The chosen servo valve has a nominal flow rate of 100 L/min, which is equivalent to the nominal flow rate specifications for the solenoid valves allowing an

opportunity for comparison. The inflow and outflow of the servo valve are also captured using the 2nd order bi-polynomial fitting function (Equation (5)) by replacing u_{duty} with u_{servo}.

2.4   System Model for Control Design

In this paper and system, the muscle actuator drives a pneumatic cylinder in a horizontal configuration resulting in additional and unknown friction. For the sliding mode control design, a continuous system model is needed and discontinuous frictional elements (static or Coulomb) are neglected in the system model. The overall model can be derived as:

$$M\ddot{x} = F_m(x, p_m) - B_{eff}\dot{x} - p_{cyl}A_{cyl} \qquad (6)$$

where F_m is the static muscle force described in Equation (1), M is the mass of moving parts (dominated by the payload mass), and p_{cyl} and A_{cyl} are the cylinder pressure and effective piston rod side area, respectively. The frictional force includes viscous friction, where $B_{eff} = 95$ Ns/m is an experimentally identified effective viscous friction factor. Coulomb and static friction that are present in the real system can be considered as modelling uncertainties and disturbances that the SMC control strategy shall compensate for. The state vector for the system studied in this paper is defined as follows:

$$\boldsymbol{x} = \begin{bmatrix} \boldsymbol{x} & \underline{\boldsymbol{x}} & \overline{\boldsymbol{x}} & \boldsymbol{p_m} \end{bmatrix}^T \qquad (7)$$

For a controller design, the following single-output (SISO) canonical form is considered:

$$\underline{\boldsymbol{x}} = F(\boldsymbol{x}) + G(\boldsymbol{x})\boldsymbol{u_{control}}, \boldsymbol{h}(\boldsymbol{x}) = \boldsymbol{x} \qquad (8)$$

where $u_{control}$ is the control input, and x is the state vector, F and G vectors and h is the output of interest (position). The actual control input (duty ratio) appears in the definition of the equivalent mass flow rate defined in Equation (4). Note that it is rather difficult to obtain equations such that it also appears in the system motion equation.

However, if the inverse of the valve flow model is used as a part of the control structure as shown in Figure 4, the equivalent mass flow rate can be defined as a control input $u_{control}$. Differentiating Equation (6) yields the following:

$$\ddot{x} = f(\boldsymbol{x}) + g(\boldsymbol{x})\boldsymbol{u_{control}}, \boldsymbol{where}$$
$$f(\boldsymbol{x}) = L_f^3 h(\boldsymbol{x}) = \frac{H\underline{\boldsymbol{x}} - B_{eff}\overline{\boldsymbol{x}}}{M}, g(\boldsymbol{x}) = L_G L_F^2 h(\boldsymbol{x}) = \frac{C}{M},$$
$$u_{control} = \dot{m}_{eq}, H = a_1 + 2a_2 x + 3a_3 x^2 + (p_{max} - p_m)k_1$$
$$- \frac{k p_m v_1}{V_m(x)}(k_0 - k_1 x), C = (k_0 - k_1 x)\frac{kRT}{V_m(x)}$$
$$\qquad (9)$$

where Equations. (1–3) are substituted into Equation (6), and rearranged as terms H and C to simplify the expression. Figure 4 illustrates the block diagram of the overall control system in single on/off valve configuration. Note, that dead-zone configuration is not used with single valve configuration, but is necessary with two valve configuration.
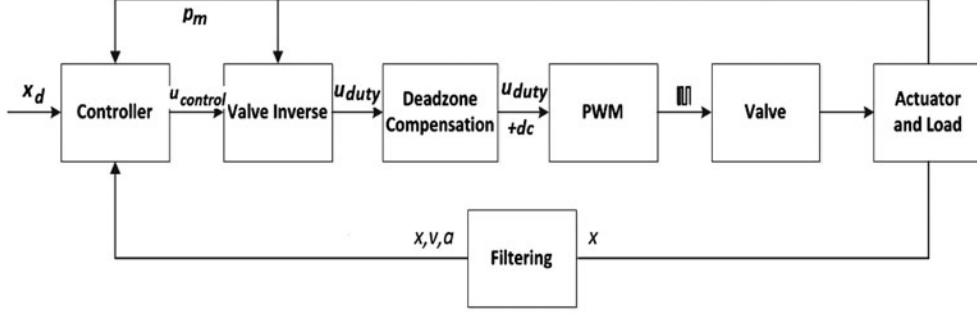
Figure 4. Block diagram of the overall control system with single on/off valve configuration.

3. Sliding Mode Control Design

SMC is a form of variable structure control that utilizes a plane in the state space termed the sliding surface (Utkin, 1978; Slotine & Li, 1991). The objective is to keep the state values close to this surface by minimizing the state errors (between the desired trajectory and the estimated or actual values). Ideally, if the state value is away from the surface, a switching gain would be used to push the state towards the sliding surface. Once on the surface, the states slide along the surface in what is called the sliding mode (Slotine & Li, 1991). The switching brings inherent stability and robustness to the control strategy, while also introducing chattering (high-frequency switching) that is undesirable in practice and can excite un-modelled dynamics. A boundary layer may be introduced within a region of the sliding surface to minimize chattering.

The order of the overall system is three. A common approach is to define a sliding surface of one degree less than the controlled system, as follows:

$$S = \left(\frac{d}{dt} + \lambda\right)^2 e = \ddot{e} + 2\lambda\dot{e} + \lambda^2 e \qquad (10)$$

where S is the sliding surface, λ is the control bandwidth and e is the position error defined by:

$$e = x - x_d \qquad (11)$$

The above definition for a sliding surface assumes a critically damped ($\xi = 1$) closed loop control dynamics. However, quite often the estimated or measured velocity can be very noisy which will affect the performance. In cases where a clean estimation of velocity and acceleration is difficult to obtain, the following alternative sliding surface definition can be used:

$$S = \ddot{e} + 2\xi\lambda\dot{e} + \lambda^2 e \qquad (12)$$

where the damping factor is defined by ξ.

Since PWM is being used with the on/off valves the equivalent control approach to SMC may be used (Slotine & Li, 1991). The equivalent control approach utilizes the system model, and the purpose of it is to keep the system state on the sliding surface once it has been reached. The state will stay on the surface when $dS/dt = 0$, which yields the equivalent control as follows:

$$u_{eq} = \frac{\dddot{x}_d - \hat{f}(\boldsymbol{x}) - 2\lambda\xi\ddot{e} - \lambda^2\dot{e}}{\hat{g}(\boldsymbol{x})}$$

$$\hat{f}(\boldsymbol{x}) = \frac{f_{min}(\boldsymbol{x}) + f_{max}(\boldsymbol{x})}{2}$$

$$\hat{g}(\boldsymbol{x}) = \sqrt{g_{min}(\boldsymbol{x})g_{max}(\boldsymbol{x})} \qquad (13)$$

$$\beta^{-1} \leq \frac{\hat{g}(\boldsymbol{x})}{g(\boldsymbol{x})} = \beta, \beta = \sqrt{\frac{g_{max}(\boldsymbol{x})}{g_{min}(\boldsymbol{x})}}$$

where $\hat{g}(\boldsymbol{x})$ and $\hat{f}(\boldsymbol{x})$ are estimates of $g(\boldsymbol{x})$ and $f(\boldsymbol{x})$, respectively. The estimate $\hat{f}(\boldsymbol{x})$ can be approximated by calculating the mean of minimum and maximum bounds of $f(\boldsymbol{x})$ based on uncertainties in the model parameters. A natural choice for estimate $\hat{g}(\boldsymbol{x})$ is the geometric mean of the upper and lower bounds while β is the gain margin of the design. The necessary condition for the reachability of the sliding surface is given by the following:

$$\frac{1}{2}\frac{d}{dt}S^2 \leq -\eta|S| \qquad (14)$$

where η is a design parameter that impacts the convergence rate of the sliding surface. In order to satisfy the condition, a switching control that accommodates the model uncertainties and disturbances (such as static friction) is defined as follows:

$$u_{sw} = -K_{SMC}sign(S) \qquad (15)$$

The switching gain K_{SMC} can be defined as a constant or as a function of upper bounds on modelling and system uncertainties as in (Slotine & Li, 1991)

$$K_{SMC} \geq \beta(F + \eta) + (\beta - 1)|u_{eq}|, F = \alpha|\hat{f}(\boldsymbol{x})| \qquad (16)$$

where F describes the estimation error on $f(\boldsymbol{x})$ with and uncertainty factor α.

A robust control law can be obtained by combining the equivalent control with the switching control:

$$u_{control} = u_{eq} + u_{sw} \qquad (17)$$

In this application both the equivalent and switching control terms are given in terms of mass flow rate. Due to finite sampling frequency and delays the state trajectory may start to chatter around the sliding surface. In order to reduce the chattering, a smoothing boundary layer φ is often introduced around the sliding surface, as follows:

$$u_{sw} = -K_{SMC}sat\left(\frac{S}{\varphi}\right) \quad (18)$$

Inside the boundary layer, the discontinuous switching function is interpolated by a continuous saturation function to avoid control signal discontinuities. Although the boundary layer design reduces the chattering effect, it no longer drives the tracking error to the origin, but to a small region around the origin. As a consequence, there exists a design conflict or trade-off between the requirements on smoothness of control signal and tracking precision.

As the SMC controller outputs the desired mass flow rate, the remaining step is to convert the controller output to a respective valve control signal. With servo valves, the valve control signal is an electrical voltage. With on/off valves, it is the duty ratio of the PWM signal. This conversion may be accomplished by using the second-order bi-polynomial fitting Equation (5) with the given values for the mass flow rates and the pressure measurement p_m. The bi-polynomial Equation (5) reduces to the following quadratic equation with u_{duty}:

$$
\begin{aligned}
&C_{21}u_{duty}^2 + C_{11}u_{duty} + C_{01} = 0 \\
&C_{01} = m_1 + m_2 p_m + m_3 p_m^2 - \dot{m}_{eqd} \\
&m_4 + m_5 p_m + m_6 p_m^2 \; C_{21} = m_7 + m_8 p_m + m_9 p_m^2 \\
&\dot{m}_{eqd} = u_{control} = u_{eq} + u_{sw}
\end{aligned}
\quad (19)
$$

The correct value for desired input signal was determined to be the most positive root, as follows:

$$u_{duty} = \frac{-C_{11} + \sqrt{C_{11}^2 - 4C_{21}C_{01}}}{2C_{21}} \quad (20)$$

In the case of two on/off valves and the servo valve, Equation (17) is solved separately for both the inflow u_{inflow} and outflow $u_{outflow}$ cases:

$$u_{inflow} = \begin{cases} 0 & u_{control} \le 0 \\ d_{min} & 0 < u_{control}, u_{duty} \le d_{min} \\ u_{duty} & 0 < u_{control}, d_{min} \le u_{duty} \end{cases} \quad (21)$$

$$u_{outflow} = \begin{cases} 0 & u_{control} \ge 0 \\ d_{min} & 0 > u_{control}, u_{duty} \le d_{min} \\ u_{duty} & 0 > u_{control}, d_{min} \le u_{duty} \end{cases}$$

where experimentally determined $d_{min} = 0.08$ is used to compensate for the dead zone of the valves as there is no flow with $u_{duty} < d_{min}$. Similarly, the control signal of the servo valve U_{servo}. with dead zone compensation $u_{dz} = 0.25$ V. is defined as:

$$U_{servo} = \begin{cases} u_0 + u_{dz} & 0 < u_{control}, u_{servo} < u_{dz} \\ u_0 + u_{servo} & 0 < u_{control}, u_{servo} \ge u_{dz} \\ u_0 - u_{dz} & 0 > u_{control}, u_{servo} < u_{dz} \\ u_0 - u_{control} & 0 > u_{control}, u_{servo} \ge u_{dz} \end{cases} \quad (22)$$

where $u_0 = 5V$ (spool in mid-position).

4. Experimental Results

Experiments were conducted to demonstrate the performance of the SMC strategy with the aforementioned valve configurations. For the implementation of the SMC strategy, the system states defined by Equation (7) are required. The velocity was obtained by differentiating the measured position signal which was then filtered by a second-order Butterworth low pass filter with a cut-off frequency of 65 Hz. The acceleration estimate was obtained by differentiating the velocity estimate, and filtering it again by a similar low-pass filter (cut-off frequency 50 Hz). The cut-off frequencies were tuned experimentally to provide the best result.

The experiments were performed for sinusoidal desired trajectories (amplitude 14mm) for frequencies of 0.25 Hz, 0.5 Hz, and 1 Hz. The cylinder force was set at 50N. With the on/off valve configurations, a PWM frequency of 100 Hz was used. Each experiment was repeated five times, and the averaged root mean square error (RMSE) values were calculated as follows:

$$RMSE = \sqrt{\frac{1}{N}\sum_{i=1}^{N} e_i^2} \quad (23)$$

where i is the current sample number, e_i is the error for the current sample, and N is the total number of samples. The experiment length of time was 8 sec with a 1000 Hz sampling rate.

4.1 Controller Tuning

Based on simulation and experimental results with a nominal payload of 2 kg, the control bandwidth was set to $\lambda = 85$ rad/s and the damping ratio was set to $\xi = 0.1$. The switching gain should be large enough to provide robustness to parameter uncertainties. Note that it also determines how quickly the system states converge towards the sliding surface. Figure 5(a) illustrates the step responses of the system with different values of K_{SMC} and control law defined by Equation (13), Equation (15) and Equation (17). In order to provide enough flow to follow a sinusoidal curve (amplitude of 14 mm at 1 Hz), K_{SMC} was set to 0.6×10^{-3} kg/s. As described earlier, excessive control chattering can be reduced by a boundary layer based control law with saturation. Figure 5(b) illustrates the tracking performance as a function of bounry layer thickness for each configuration: single on/off valve, dual on/off valves, and a servo valve.

In Figure 5(b), the *total RMSE* is defined as the sum of RMSE values for sinusoidal input frequencies 0.25 Hz, 0.5 Hz, and 1 Hz. For every valve configuration, the boundary layer width improves the tracking performance up to a certain point, after which the control accuracy begins to degrade.

It is also interesting to note that the system with two on/off valves can provide a better tracking

(a) Switching gain variation

(b) Boundary layer thickness variation
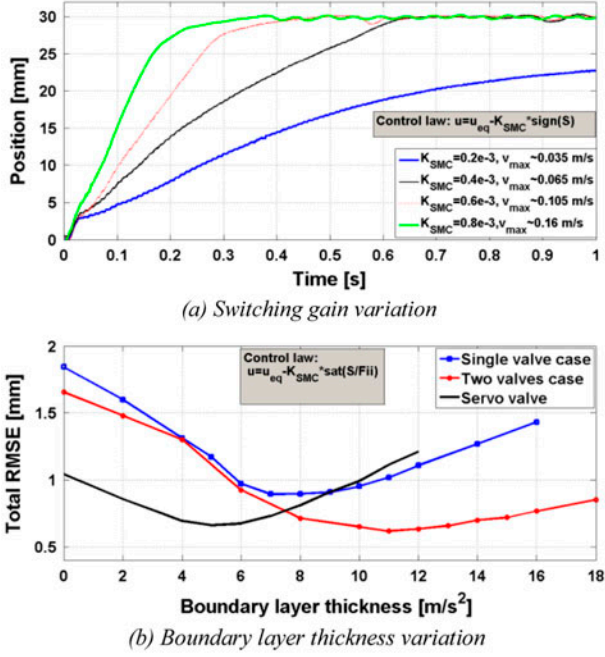
Figure 5.   Determination of important control parameters.

Table 2.   Comparison of RMSE values [mm] averaged over five tests for the three valve configurations (as per Figures 6 and 7).

Frequency	Single On/Off	Dual On/Off	Servo Valve
0.25 Hz	0.196	**0.087**	0.091
0.5 Hz	0.268	**0.170**	0.205
1 Hz	0.448	0.378	**0.367**
Total RMSE	0.912	**0.635**	0.663

performance than the system with the servo valve. This is assumed to be caused by the friction in the system as the PWM switching decreases the static friction of the system. The boundary layer thickness values are chosen based on the these curves and the amount of control signal chattering resulting in $\varphi = 9$ for single valve; $\varphi = 12$ for two on/off valves; and $\varphi = 5$ for the servo valve.
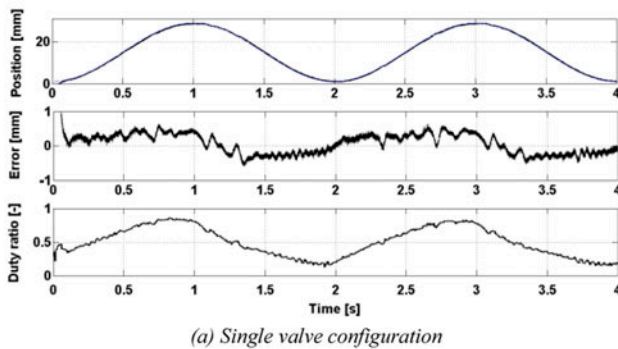
4.2   Sinusoidal Tracking (Normal Conditions)

Table 2 lists the mean RMSE values for the valve configurations with sinusoidal tracking and the nominal payload. As demonstrated by these results, the dual valve configuration provides the best tracking with sinusoidal frequencies 0.25 Hz and 0.5 Hz. The dual valve and servo valve configurations improve the tracking performance up to 30% when compared with the single on/off valve case. It is also notable that the tracking performance with the dual valve configuration is slightly better than compared to the servo valve system (overall). Figure 6 illustrates the performance for sinusoidal tracking at 0.5 Hz for the single valve and dual valve configurations. The performances for sinusoidal tracking at 1Hz for the dual valve and servo valve configurations are shown in Figure 7.

Note that slight oscillations occur in the control performance during the negative direction movement. This may be due to the cylinder acting like a driving force, and the muscle actuator acting like a brake; which is more difficult to control as the air is released from the actuator. Finally, note also that the magnitude of the oscillation is smaller in the servo valve system due to its faster sampling rate.

4.3   Robustness to Payload Variation

The RMSE results of this section are summarized in Tables 3 and 4. The payload was decreased to $M = 0.5$ kg and also increased to $M = 4$ kg. It is interesting to observe that the on/off valve configurations are extremely robust to decreased payload mass as the total RMSE is actually improved when compared with the nominal case. Conversely, the total RMSE of the servo valve configuration increases with payload mass $M = 0.5$ kg by approximately 37% when compared with the nominal case. This is most likely due to the control effort being excessive for the decreased inertia which leads to increased chattering around the sliding surface.

For the second payload variation ($M = 4$ kg), the performance of the case with two on/off valves degrades 79% on average, and 46% with the single valve

(a) Single valve configuration

(b) Dual valve configuration
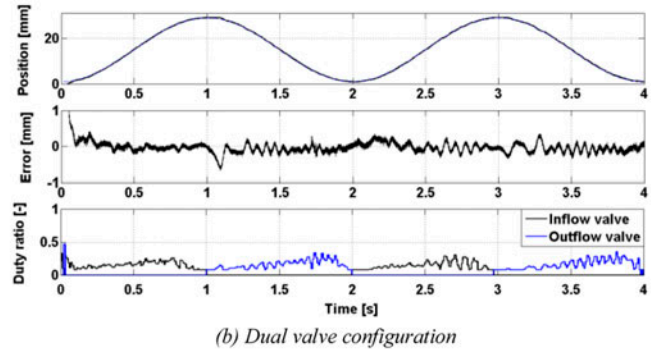
Figure 6.   Sinusoidal tracking (at 0.5 Hz with $M = 2$ kg).

(a) Dual valve configuration

(b) Servo valve configuration
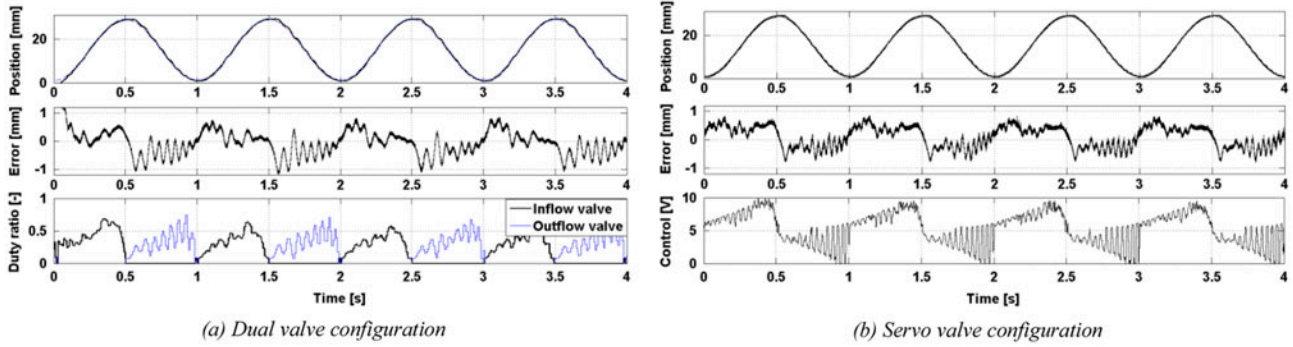
Figure 7.   Sinusoidal tracking (at 1 Hz with $M = 2$ kg).

Table 3.   Comparison of average RMSE [mm] with payload $M = 0.5$ kg (as per Figure 9).

Frequency	Single On/Off	Two On/Off	Servo Valve
0.25 Hz	0.163	**0.079**	0.135
0.5 Hz	0.230	**0.142**	0.232
1 Hz	0.470	**0.354**	0.543
Total RMSE	0.863	**0.575**	0.910

Table 4.   Comparison of average RMSE [mm] with payload $M = 4$ kg (as per Figure 9).

Frequency	Single On/Off	Two On/Off	Servo Valve
0.25 Hz	0.231	0.193	**0.131**
0.5 Hz	0.356	0.313	**0.209**
1 Hz	0.748	0.633	**0.434**
Total RMSE	1.335	1.139	**0.774**

compared with the nominal case. In terms of robustness, the best performance with the increased payload mass is obtained with the servo valve configuration, as the total RMSE increases by only 16%. With all of the valve configurations, oscillations occurred in the motion signal with increased inertia. This is due to a relatively low damping ratio $\xi = 0.1$ of the closed loop control

dynamics, which begins to affect the performance as the inertia of the system increases.

Figure 8 illustrates the damping ratio effect on the control performance with the nominal payload mass $M = 2$ kg and increased payload mass $M = 4$ kg with each system configuration. The calculated tracking accuracy is the sum of the RMSE values with sinusoidal inputs 0.25 Hz and 0.5 Hz. With the nominal payload $M = 2$ kg, the tracking performance degrades significantly while increasing the damping ratio. A higher damping ratio magnifies the noise in the system, which results in poor performance, especially when studying the on/off valve configurations. The servo valve configuration has a faster control loop, which provides better robustness to increased noise. Under the $M = 4$ kg condition, the systems start to oscillate when low damping ratios are implemented, thus a higher damping ratio is needed. The best performance is obtained by using a damping ratio of 0.4 with the servo valve and two valves systems, and 0.7 with the single valve system. Note also that a high damping ratio decreases the tracking accuracy which can be seen amongst all of the configurations.

Figure 9 illustrates the effect of the damping ratio on the performances of the two valves and servo valve configurations. As stated earlier, it is observed that the servo valve configuration provides a much better damping of oscillations due to the faster control loop. With the

(a) Effect with $M = 2$ kg
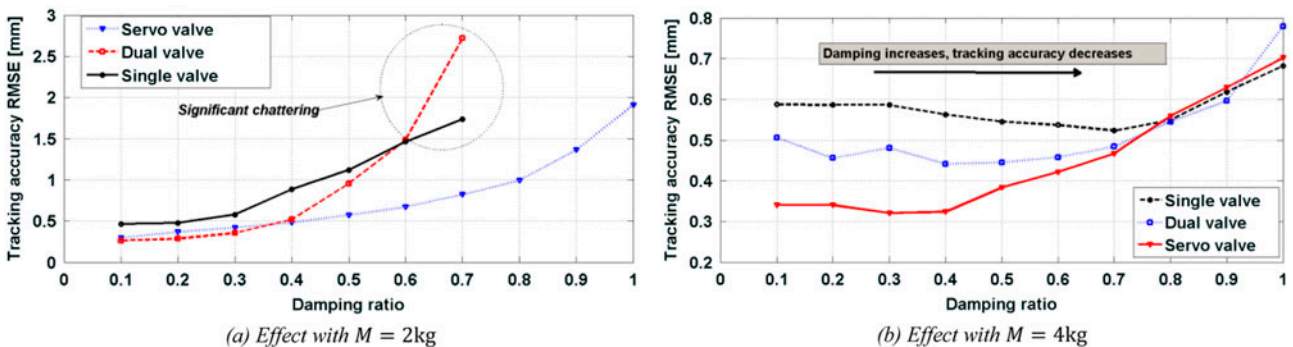
(b) Effect with $M = 4$ kg

Figure 8.   Effect of damping ratio (dr) with various payloads (M = 2 kg and M = 4 kg).

(a) Two valve configuration   (b) Servo valve configuration
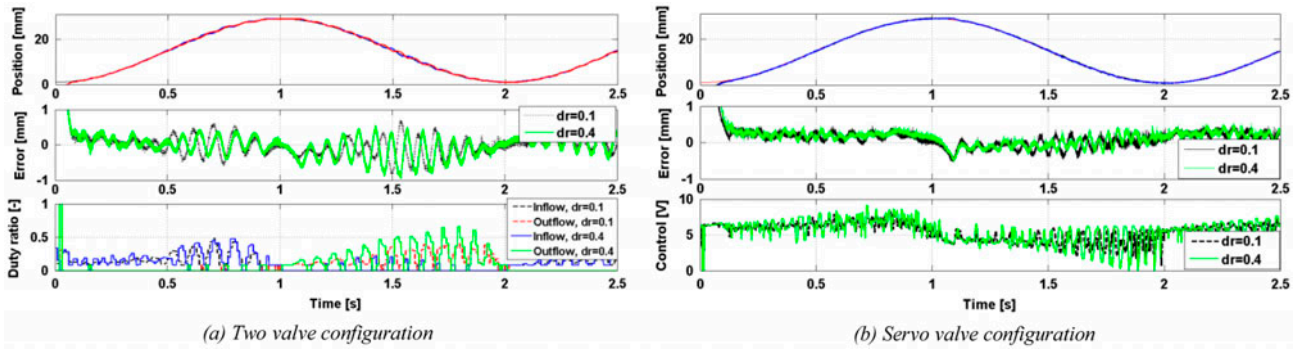
Figure 9. Sinusoidal tracking (at 0.5 Hz with M = 4 kg).

Table 5. Comparison of average RMSE [mm] with external disturbance (as per Figure 10).

Disturbance	Single On/Off	Two On/Off	Servo Valve
1 Hz (Sine)	0.173	0.149	**0.120**
2 Hz (Sine)	0.288	0.238	**0.178**
0.75 Hz (Step)	0.280	0.237	**0.177**
None	0.123	**0.083**	0.097

PWM-actuated on/off valve systems, the PWM sampling introduced unwanted delay decreases the overall robustness of the SMC strategy.

4.4 Robustness to External Disturbances

Robustness to external disturbances was tested by applying sinusoidal and square wave force profiles with the pneumatic cylinder. The amplitude of the force disturbance was 25 N and the mean value was 50 N. Frequencies of 1 Hz and 2 Hz were used for the sinusoidal disturbance, and 0.75 Hz for the square wave disturbance.

Table 5 summarizes the RMSE values when the desired trajectory is sinusoidal with an amplitude of 10 mm at 0.25 Hz. Although each of the valve configurations is capable of providing a reasonable response for the applied disturbance signals, the best performance is obtained with the servo valve configuration. Figure 10 illustrates the tracking performance of the two valves and servo valve systems, with sinusoidal (2 Hz) and square wave (0.75 Hz) disturbances.

As illustrated by the results for the sinusoidal disturbance, the two valve system has a maximum tracking error of ±0.75 mm, whereas the servo valve system error is in the range of roughly ±0.5 mm. For the stepwise

(a) Two valve configuration (2 Hz sinusoidal disturbance)   (b) Servo valve configuration (2 Hz sinusoidal disturbance)

(c) Two valve configuration (0.75 Hz stepwise force disturbance)   (d) Servo valve configuration (0.75 Hz stepwise force disturbance)
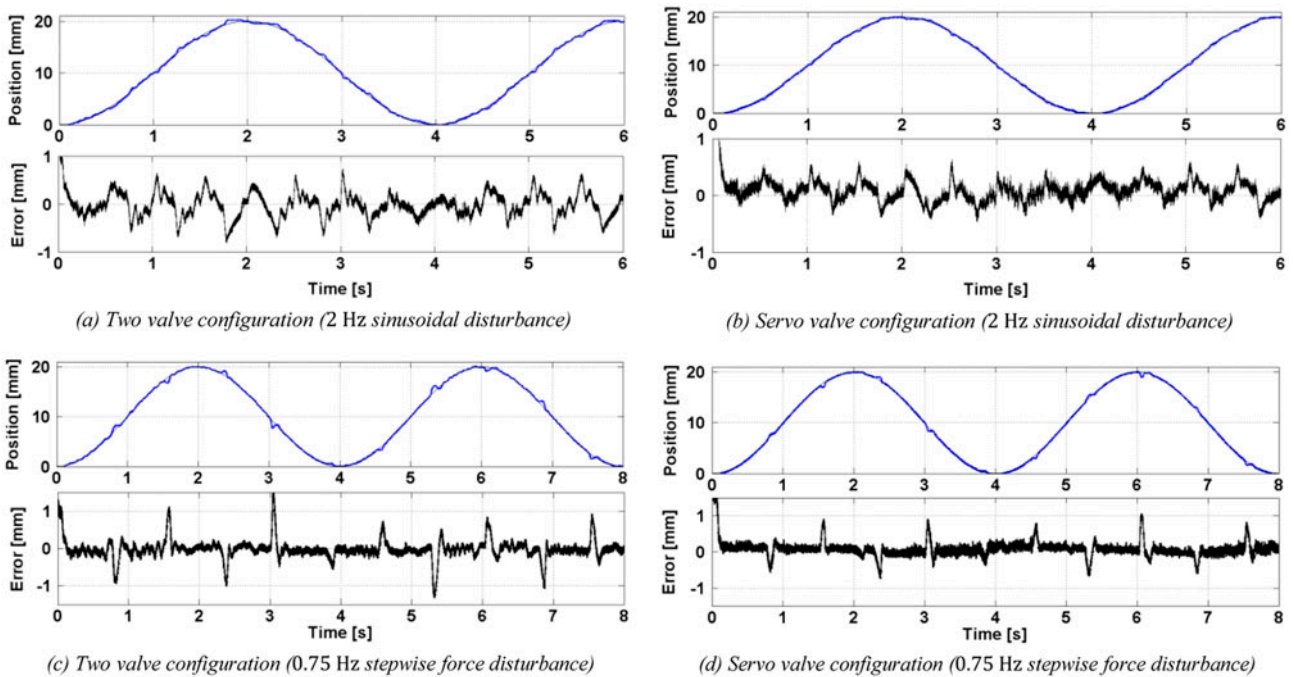
Figure 10. Sinusoidal tracking (0.25 Hz) performance with various disturbances (with M = 2 kg).

disturbance, the respective errors are about ±1.4 mm and ±1 mm. Based on these results, due to a faster control loop, the servo valve configuration provides the best response to the studied external disturbances.

5. Conclusions

This paper provides a low cost approach to control pneumatic systems by using high-speed on/off valves, instead of costly proportional and servo valves. A full nonlinear system model was derived and provided for use with PWM-driven pneumatic applications. The valve model (pressure and flow dynamics) is continuous and invertible, such that an equivalent control method such as a SMC strategy may be implemented. A comparison of three valve configurations was made: single on/off valve, two on/off valves, and a servo valve. In nominal conditions, the two valves and servo valve configurations are capable of providing a 30% reduction in RMSE compared with the single on/off valve case. In general, the two valve system provided slightly better tracking accuracy compared with the servo valve system.

The robustness of the control configurations was tested by changing the payload mass and by applying an external force disturbance. When decreasing the payload mass, the two on/off valves configuration was the most robust. However, when increasing the payload mass, the servo valve configuration provided the best results. Against external force disturbances, the servo valve also provided the best robustness. Overall, the PWM-actuated on/off valve controlled muscle actuator system provided a low cost option with a performance almost similar to servo valve controlled systems.

Nomenclature

Symbol	Description	Unit
A_{cyl}	cylinder effective piston rod side area	[m²]
b	Critical pressure ratio	[−]
B_{eff}	Effective viscous friction	[Ns/m]
C	Valve conductance	$\left[\frac{kg}{sMPa}\right]$
d_{min}	Min. duty ratio to provide flow	[−]
f_{PWM}	PWM frequency	[Hz]
F_m	Muscle actuator force	[N]
F_{max}	Max. muscle actuator force	[N]
k	Specific heat ratio	[−]
K_{SMC}	Switching gain	[kg/s]
$\dot{m}$	Mass flow rate	[kg/s]
$\dot{m}_{eq}$	Equivalent mass flow rate	[kg/s]
M	Payload mass	[kg]
p_{cyl}	Cylinder pressure	[Pa]
p_{down}	Downstream pressure	[Pa]
p_m	Muscle actuator pressure	[Pa]
p_{max}	Max. muscle actuator pressure	[Pa]
p_s	Supply pressure	[Pa]
p_{up}	Upstream pressure	[Pa]
p_0	Atmosphere pressure	[Pa]

(*Continued*)

(*Continued*).

Symbol	Description	Unit
R	Gas constant	[J/(kgK)]
S	Sliding surface	[m/s²]
T	Air temperature	[K]
$u_{control}$	Control input	[kg/s]
u_{duty}	PWM duty ratio	[−]
u_{dz}	Valve dead zone compensation	[−]
u_{eq}	Equivalent control term	[kg/s]
u_{inflow}	Duty ratio for inflow valve	[−]
$u_{outflow}$	Duty ratio for outflow valve	[−]
u_{sw}	Switching control term	[kg/s]
U_{servo}	Servo valve control signal	[V]
V_m	Muscle actuator volume	[m³]
x	Position of the actuator	[m]
x_d	Desired position	[m]
α	Uncertainty factor	[−]
β	Gain margin	[−]
η	Control design parameter	[m/s³]
λ	Control bandwidth	[rad/s]
ξ	Damping factor	[−]
φ	Boundary layer width	[m/s²]

The following is a list of important parameters used with corresponding definitions and values, where applicable.

Parameter	Value
a_0	$484\,[N]$
a_1	$-1.97e4\,[N/m]$
a_2	$4.34e5\,[N/m^2]$
a_3	$-4.33e6\,[N/m^3]$
k	1.4
k_0	$0.00079\,[N/Pa]$
k_1	$0.00751\,\left[\frac{N}{Pa}m^{-1}\right]$
m_1	$-2.26 \times 10^{-4}\,[kg/s]$
m_2	$-3.05 \times 10^{-9}\,[kg/sPa]$
m_3	$-3.3 \times 10^{-15}\,[kg/sPa^2]$
m_4	$0.002\,[kg/s]$
m_5	$5.35 \times 10^{-9}\,[kg/sPa]$
m_6	$-2.35 \times 10^{-15}\,[kg/sPa^2]$
m_7	$6.01 \times 10^{-4}\,[kg/s]$
m_8	$-1.5 \times 10^{-9}\,[kg/sPa]$
m_9	$-1.62 \times 10^{-15}\,[kg/sPa^2]$
B_{eff}	$95\,[Ns/m]$
M	$2\,[kg]$
p_{max}	$0.6\,[MPa]$
R	$287\,[J/(kgK)]$
T	$293\,[K]$
v_0	$2.4 \times 10^{-5}\,[m^3]$
v_1	$5.6 \times 10^{-4}\,[m^2]$

Notes on contributors

Ville T. Jouppila (M.Sc '05, TUT) is currently pursuing his PhD degree and working as a Research Scientist at the Department of Mechanical Engineering and Industrial Systems at Tampere University of Technology (TUT) in Finland. His research interests include advanced control systems in Mechatronics and Fluid Power, advanced actuator technologies, and model-based systems engineering.

S. Andrew Gadsden Andrew obtained his Ph.D. in the area of state and parameter estimation theory in 2011 from the Department of Mechanical Engineering at McMaster University, Canada. His work involved an optimal realization and further advancement of the smooth variable structure filter (SVSF). His background includes a broad consideration of state and parameter estimation strategies, the variable structure theory, fault detection and diagnosis, mechatronics, target tracking, cognitive systems, and neural networks. He is the recipient of a number of professional and scholarly awards, and is currently a postdoctoral Fellow at McMaster. Andrew is an Associate Editor of the Transactions of the Canadian Society for Mechanical Engineering, and is a member of the Professional Engineers of Ontario (PEO) and the Ontario Society of Professional Engineers (OSPE). He is also a member of the American Society of Mechanical Engineers (ASME) and the Institute of Electrical and Electronics Engineers (IEEE).

Gary M. Bone received his B.Sc. (Ap.Sc.) degree from the Department of Mechanical Engineering, Queen's University, Canada, and his M.Eng. and Ph.D. degrees from McMaster University in 1986, 1988, and 1993, respectively. He joined the Faculty of Engineering at McMaster University in 1994, where he is currently a Professor in the Department of Mechanical Engineering. His research interests include: servo pneumatic actuators, robot design, robot control, and machine vision.

Asko U. Ellman (M.Sc '85, PhD '92, TUT) is a Professor at the Department of Mechanical Engineering and Industrial Systems. He is the leader of Virtual Design research group. His research interests include Virtual Design, Mechatronics and Fluid Power.

Saeid R. Habibi Saeid is currently Director of the Centre for Mechatronics and Hybrid Technology and a Professor in the Department of Mechanical Engineering at McMaster University. Saeid obtained his Ph.D. in Control Engineering from the University of Cambridge, U.K. His academic background includes research into intelligent control, state and parameter estimation, fault diagnosis and prediction, variable structure systems, and fluid power. The application areas for his research have included aerospace, automotive, water distribution, robotics, and actuation systems. He spent a number of years in industry as a Project Manager and Senior Consultant for Cambridge Control Ltd, U.K., and as Senior Manager of Systems Engineering for AlliedSignal Aerospace Canada. He received two corporate awards for his contributions to the AlliedSignal Systems Engineering Process in 1996 and 1997. He was the recipient of the Institution of Electrical Engineers (IEE) F.C. Williams best paper award in 1992 for his contribution to variable structure systems theory. He was also awarded an NSERC Canada International Postdoctoral Fellowship that he held at the University of Toronto from 1993 to 1995, and more recently a Boeing Visiting Scholar sponsorship for 2005. Saeid is on the Editorial Board of the Transactions of the Canadian Society of Mechanical Engineers and is a member of IEEE, ASME, and the ASME Fluid Power Systems Division Executive Committee

References

anon. (2005). ISO-6358 Pneumatic Fluid Power - Components Using Compressible Fluids - Determination of Flow-Rate Characteristics. International Organization for Standardization. Geneve.

Ahn, K., & Yokota, S. (2005). Intelligent Switching Control of Pneumatic Actuator using On/Off Solenoid Valves. *Mechatronics, 15*, 683–702.

Aschemann, H., & Schindele, D. (2008). Sliding-mode Control of a High-Speed Linear Axis Driven by Pneumatic Muscle Actuators. *IEEE Transactions on Industrial Electronics, 11* (55), 3855–3864.

Balasubramanian, K., & Rattan, K. S. (2003). Feedforward Control of a Nonlinear Pneumatic Muscle System Using Fuzzy Logic. *IEEE International Conference of Fuzzy Systems, 1*, pp. 272–277.

Barth, E. J., Zhang, J., & Goldfarb, M. (2003). Control Design for Relative Stability in a PWM-Controlled Pneumatic Systems. *ASME Journal of Dynamic Systems, Measurement and Control, 125*(3), 504–508.

Caldwell, D. G., Medrano-Cerda, G. A., & Goodwin, M. J. (1995). Control of Pneumatic Muscle Actuators. *IEEE Control Systems Magazine, 15*, No.1, pp. 40–48.

Carbonell, P., Jiang, Z. P., & Repperger, D. W. (2001). Nonlinear Control of a Pneumatic Muscle Actuator: Backstepping vs. Sliding Mode. *Proceedings of the IEEE International Conference on Control Applications*, (pp. 167–172).

Chan, S. W., Lilly, J. H., Repperger, D. W., & Berlin, J. E. (2003). Fuzzy PD+I Learning Control for a Pneumatic Muscle. *Proceedings of 2003 IEEE International Conference on Fuzzy Systems*, (pp. 278–283). St Louis, USA.

Chou, P., & Hannaford, B. (1996). Measurement and Modeling of a McKibben Pneumatic Artificial Muscles. *IEEE Transaction on Robotics and Automation, 12*(1).

Gaylord, R. H. (1958). *Patent No. 2,844,126*. U.S.A.

Hesselroth, T., Sarkar, K., Van der Smagt, P., & Schulten, K. (1994). Neural Network Control of a Pneumatic Robot Arm. *IEEE Transaction of Systems, Man and Cybernetics, 24, No.*1, pp. 28–38.

Jouppila, V. T., Gadsden, S. A., & Ellman, A. U. (2010). Modeling and Identification of a Pneumatic Muscle Actuator System Controlled by an On/Off Solenoid Valve. *Proceedings of 7th International Fluid Power Conference*, (p. 16). Aachen, Germany.

Lai, J. Y., Singh, R., & Menq, C. H. (1992). Development of PWM mode Position Control for a Pneumatic Servo System. *Journal of the Chinese Society of Mechanical Engineers, 13*(1), 86–95.

Lilly, J. (2003). Adaptive Tracking for Pneumatic Muscle Actuators in Bicep and Tricep Configurations. *IEEE Transaction of Neural Systems and Rehabilitation Engineering, 11*, No. 3, pp. 333–339.

Lilly, J. H., & Yang, L. (2005). Sliding Mode Tracking for Pneumatic Muscle Actuators in Opposing Pair Configuration. *IEEE Transactions on Control Systems Technology, 13*, pp. 550–558.

Medrano-Cerda, G. A., Bowler, C. J., & Caldwell, D. G. (1995). Adaptive Position Control of Antagonistic Pneumatic Muscle Actuators. *IEEE/RSJ International Conference on Intelligent Robots and Systems, 1*, pp. 378–383. Pittsburgh.

Morita, Y. S., Shimizu, M., & Kagawa, T. (1985). An Analysis of Pneumatic PWM and Its Application to a Manipulator. *Proceedings of International Symposium of Fluid Control and Measurement*, (pp. 3–8). Tokyo, Japan.

Nguyen, T., Leavitt, J., Jabbari, F., & Bobrow, J. E. (2007, April). Accurate Sliding-Mode Control of Pneumatic Systems Using Low-Cost Solenoid Valves. *IEEE/ASME Transactions on Mechatronics, 12*(2), 216–219.

Noritsugu, T. (1986). Development of PWM Mode Electro-Pneumatic Servomechanism, Part I: Speed Control of a Pneumatic Cylinder. *Journal of Fluid Control, 17-1*, 65–80.

Paul, A. K., Mishra, J. K., & Radke, M. G. (1994). Reduced Order Sliding Mode Control for Pneumatic Actuator. *IEEE Transaction on Control Systems Technology, 2*(30), 271–276.

Rao, Z., & Bone, G. M. (2008). Nonlinear Modeling and Control of Servo Pneumatic Actuators. *IEEE Transactions on Control Systems Technology, 16*, 562–569.

Schulte, R. A. (1962). The Characteristics of the McKibben Artificial Muscle. *The Applications of External Power in Prosthetics and Orthotics*, 94–115.

Shen, X. (2010). Nonlinear Model-Based Control of Pneumatic Artificial Muscle Actuator Systems. *Control Engineering Practice, 18*, 311–317.

Shen, X., Zhang, J., Barth, E., & Goldfarb, M. (2006). Nonlinear Model-Based Control of Pulse Width Modulated Pneumatic Servo Systems. *ASME Journal of Dynamic Systems, Measurement and Control, 128*, 663–669.

Slotine, J. J., & Li, W. (1991). *Applied Nonlinear Control*. Englewood Cliffs, New Jersey, USA: Prentice-Hall.

Than, T., & Ahn, K. (2006). Nonlinear PID Control to Improve the Control Performance of 2 Axes Pneumatic Artificial Muscle Manipulator Using Neural Networks. *Mechatronics, 16*, 577–587.

Tondu, B., & Lopez, P. (2000). Modeling and Control of McKibben Artificial Muscle. *IEEE Control Systems Magazine*, (pp. 15–38).

Utkin, V. I. (1978). *Sliding Modes and Their Application in Variable Strucure Systems*. Moscow, Russia: MIR Publishers.

Van Varseveld, R. B., & Bone, G. M. (1997). Accurate Position Control of a Pneumatic Actuator Using On/Off Solenoid Valves. *IEEE/ASME Transaction on Mechatronics, 2*(30), 195–2004.